AIP | Review of Scientific Instruments

Development of a precision nanoindentation platform

B. K. Nowakowski, D. T. Smith, S. T. Smith, L. F. Correa, and R. F. Cook

Citation: Rev. Sci. Instrum. **84**, 075110 (2013); doi: 10.1063/1.4811195
View online: http://dx.doi.org/10.1063/1.4811195
View Table of Contents: http://rsi.aip.org/resource/1/RSINAK/v84/i7
Published by the AIP Publishing LLC.

Additional information on Rev. Sci. Instrum.

Journal Homepage: http://rsi.aip.org
Journal Information: http://rsi.aip.org/about/about_the_journal
Top downloads: http://rsi.aip.org/features/most_downloaded
Information for Authors: http://rsi.aip.org/authors

ADVERTISEMENT

REVIEW OF SCIENTIFIC INSTRUMENTS **84**, 075110 (2013)

Development of a precision nanoindentation platform

B. K. Nowakowski,[1] D. T. Smith,[1,a)] S. T. Smith,[2] L. F. Correa,[1] and R. F. Cook[1]
[1]*Nanomechanical Properties Group, Material Measurement Laboratory, National Institute of Standards and Technology, Gaithersburg, Maryland 20899, USA*
[2]*Center for Precision Metrology at UNC Charlotte, Charlotte, North Carolina 28223, USA*

(Received 22 February 2013; accepted 28 May 2013; published online 18 July 2013)

The design, construction, and performance of a surface-referenced nanoindentation instrument, termed a precision nanoindentation platform (PNP), are presented. The PNP is a symmetrically designed instrument with a centrally located indenter tip attached to a force cell for measuring the forces between the tip and a specimen. Penetration of the indenter tip into the specimen surface is measured using two proximity sensors placed symmetrically about the indenter. Each proximity sensor is attached to a piezoelectric actuator that is servo controlled to maintain the sensor and the reference frame to which it is attached at a constant height relative to the specimen surface. As the indenter tip penetrates the specimen surface, the movement of the tip relative to the two surface reference frames is measured using capacitance gauges and the average of these displacements is used as a measure of penetration depth. The current indenter is capable of applying indentation forces of up to 150 mN with a noise floor below 2 μN rms for a sampling rate of 1 kHz, and measuring displacement with 0.4 nm rms noise for the same sampling rate. The proximity sensors are capable of maintaining surface height variations of less than 1.0 nm with penetration depths of up to 10 μm. Long-term stability tests indicate a total uncertainty in indentation depth less than 10 nm for periods as long as 12 h. To demonstrate instrument accuracy, repeated indention cycles were performed on a fused silica specimen using incrementally increasing indention force. From this test, an average value of 72 GPa ± 1.5 GPa for the Young's modulus was obtained from the elastic unloading curves for 10 measurements ranging in maximum force from 5 mN to 50 mN. To demonstrate longer-term instrument stability, a poly(methyl methacrylate) specimen was subjected to a fixed 5 mN indentation force for 4 h; two distinct creep-like mechanisms were observed. © *2013 AIP Publishing LLC*.
[http://dx.doi.org/10.1063/1.4811195]

I. INTRODUCTION

As the sizes of indentations in nanohardness testing reduce to nanometer scales, for most practical measurements it becomes necessary to measure the indenter penetration into the surface rather than the impression area commonly used for large indentations.[1] A continuous record of the force and indenter penetration distance can also provide data to extract further information about the elastic and geometric properties of the indentation. During early nanoindentation tests it was realized that, because force and measurement loops typically followed the same path around the instrument, compliances in coincident loop components represented a major source of uncertainty.[2,3] To address this issue, a number of researchers have explored indenter designs that measure penetration of the indenter tip into the surface by directly measuring displacement of the indenter housing relative to, or from, a target immediately adjacent to, the specimen surface. Some of these designs are discussed below.

To obtain indentation depth information on metal surfaces at known penetration depths Howes *et al.*[4] in 1987 deposited an electrode coating onto a diamond indenter tip. By subsequently indenting into a steel surface at a load of 9.8 N, the coating was removed to a fixed distance from the tip apex. With such a tip it was possible to make indentations until an electrical contact was established. While, in principal, this should enable indentations of fixed depth, issues such as electrode wear, metal pile-up during indentation, and coating uniformity resulted in considerable measurement uncertainty. This same group explored another method to use the tip itself as a surface area transducer by measuring the contact resistance of either a silicon carbide[5] or a semiconductor diamond indenter.[6] While reproducible measurements were demonstrated, there was considerable variability in hardness measurements when used at arbitrary loads and this approach does not appear to have been pursued further.

The first indenter that recorded indentation depths referenced to the surface was demonstrated by Daniel *et al.*,[7] in 1994. This was a relatively simple design that used a capacitance based cantilever stylus gauge that was placed immediately beside the indenter tip to measure displacement of the specimen surface relative to the common stylus and the indenter mount. To translate the indenter toward the specimen surface, the complete indenter head was attached to an inchworm translation stage housed within an electron microscope. While indentation depths of fractions of a micrometer were demonstrated, this instrument was used primarily for push-in testing of metallic fiber matrix composites with loads of up to 6 N and indenter tip radii ranging from 1 μm to 10 μm. Issues raised by this design were the Abbé offset between the indenter and the displacement gauge, the force

a)Author to whom correspondence should be addressed. Electronic mail: douglas.smith@nist.gov

 © 2013 AIP Publishing LLC

produced by the displacement sensor that might produce surface deformation, and the fact that the load cell was in the measurement loop. As a consequence of this last feature any load cell deformations (thought to be insignificant) would manifest as indenter penetration into the surface. A year later, Woirgard and Dargenton[8] presented an inverted design that measured indentation depths directly from the surface of the specimen support using an array of four coplanar capacitance electrodes sensing a common target. These four sensors could be used to determine rotation of the load cell or indenter frame; in principle, these parasitic rotations could be corrected. Force was generated by applying a high voltage to these same electrodes; these forces would transfer to the indenter and its silica support flexure. This symmetric design was capable of producing sub-nanometer indentation depth information with applied loads ranging from 0.1 μN to 100 mN. A detailed assessment of instrument uncertainties was not provided.

In 1997, Shimamoto and Tanaka[9] presented a nanoindenter design containing many of the features of that presented in Daniel *et al.* However, in this design, the load cell was incorporated into the specimen support stage and feedback for the indenter displacement measurement was obtained from a target surface immediately adjacent to the specimen. At about this time, Coley[10] designed a monolithic version of the indenter of Daniel *et al.* in which the load cell and displacement sensor support, and adjustment mechanism, were machined from a monolithic invar flexure. To measure penetration of the adjacent indenter, a blunt stylus on a cantilever beam with beam deflection measured by a capacitance sensor was used. With the stylus directly in contact with the specimen surface, this instrument was able to resolve forces and displacements with nanometer and micronewton resolution, respectively. This design retained issues associated with the design of Daniel *et al.* in which there was a varying contact load at the stylus contact during measurement and an Abbé offset between the displacement measurement and indenter contact, a feature shared by the design of Shimamoto and Tanaka.

To address the issue of the varying contact load, a variant on the design of Coley in which the surface probe was mounted into a piezoelectrically actuated translation stage with capacitance based sensing used to measure the vertical displacement of the stylus was introduced by Ellis and coworkers.[11,12] In this design, a piezoresistive atomic force microscope (AFM) cantilever was used to monitor contact of the cantilever tip (or stylus) with the specimen surface. During an indentation, this tip was first contacted with the specimen surface and subsequently servo controlled to maintain constant deformation of the cantilever beam and, by implication, constant force between the AFM stylus and specimen surface during indentation. With this design, the AFM mount is effectively maintained at a constant height above the specimen during indentation. A capacitance displacement sensor is used to measure displacement of the indenter relative to the specimen surface. Effectively, this transfers displacement sensing to the capacitance gauge of the instrument, with the AFM probe providing only a null signal for the servo control. This modular unit comprising surface reference AFM and indenter displacement sensing was then housed in a flexure connected to the indentation translation stage. A second capacitance sensor was then used, via calibration of the flexure stiffness, to independently measure indenter load. Calibration of the surface probes for displacement sensitivity can be achieved using the indenter itself, while reasonable estimates for AFM or stylus cantilever compliance can be obtained either from manufacturer's specifications, beam bending theory or via thermal noise measurement.[13–15] Controller errors during an indentation provide a measure of the force and displacement uncertainties. A similar design was presented in the patent of Woirgard *et al.*[16] and by Nohava *et al.*[17]

In this paper, we present the design and preliminary characterization of a new nanoindentation instrument that has been built at the National Institute of Standards and Technology (NIST), in collaboration with the Center for Precision Metrology at the University of North Carolina, Charlotte. This instrument, referred to as a precision nanoindentation platform (PNP), is intended to serve as a metrological instrumented indenter for purposes such as certifying NIST standard reference materials and generating standard reference data for users of commercial nanoindentation instruments, as well as providing indentation force and displacement data that are directly traceable to the International System of Units (SI), in support of a broad range of materials research.

II. INSTRUMENT DESIGN AND OPERATING PRINCIPLES

The NIST PNP is shown in Figure 1(a). It consists of a base plate that supports X-, Y-, and Z-axis (Z is vertical) coarse translation stages for positioning an indentation specimen under the indenter tip, a gantry that supports an indentation load head, and an optical microscope with video camera for examination of specimen surfaces and selection of indentation locations. The PNP is housed in a vacuum chamber, and is capable of operating in laboratory air at ambient room pressure, under inert gas over a range of pressures, or under vacuum conditions with pressure as low as 10^{-2} Pa ($\approx 10^{-4}$ Torr). A close-up of the load head is shown in Figure 1(b).

Key components of the PNP load head are shown in Figure 2. The outer frame, the D-frame, the center column, the surface tracking reference frame, and all connecting flexures have been machined from a single block of aluminum. Key items to note in Figure 2 are that (a) an indentation is performed by moving the D-frame downward with a preloaded piezoelectric actuator mounted between the outer frame and the D-frame, (b) force is determined through deflection of the flexures that connect the D-frame to the center column, and (c) displacement is measured using capacitance gauges that measure the relative motion between the center column and the surface tracking reference frames. The indenter tip is mounted to the center column via a pre-loaded clamp, through an opening in the base of the D-frame.

Two tuning forks, equally spaced $\approx$5 mm on either side of the indenter tip, interact with the specimen surface before the indenter tip makes contact. At large separations, as the tips of the tuning fork tines approach the specimen surface, the weak attractive surface interaction decreases the resonant frequency of the tuning forks (which is nominally 32 kHz in

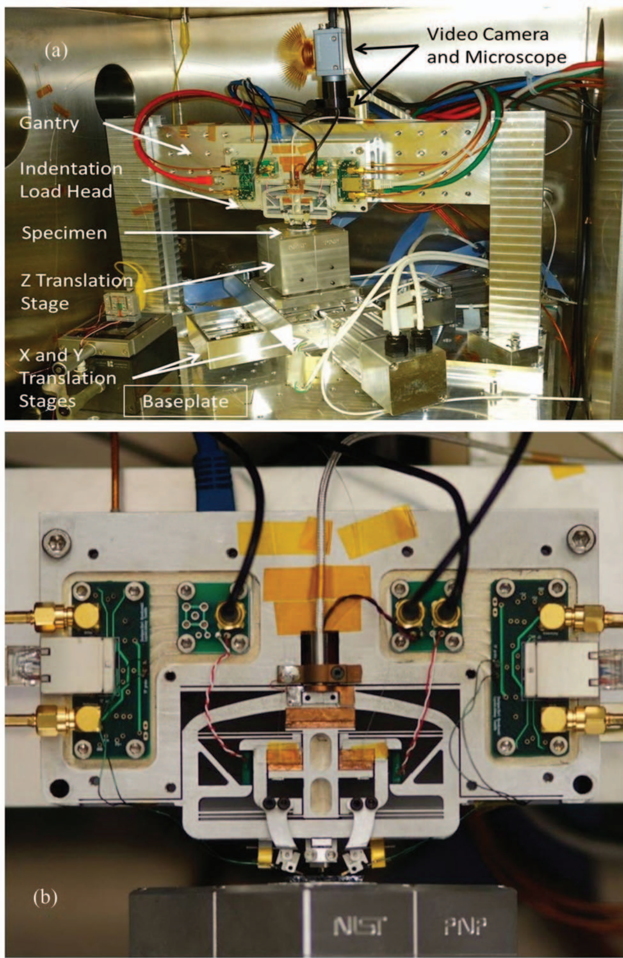

FIG. 1. (a) The interior of the PNP vacuum chamber, showing the X, Y, and Z coarse specimen positioning stages as well as the gantry and load head. (b) A close-up of the PNP load head, showing some of the electronics associated with the capacitance gauges, tuning fork sensors, and piezoelectric actuators.

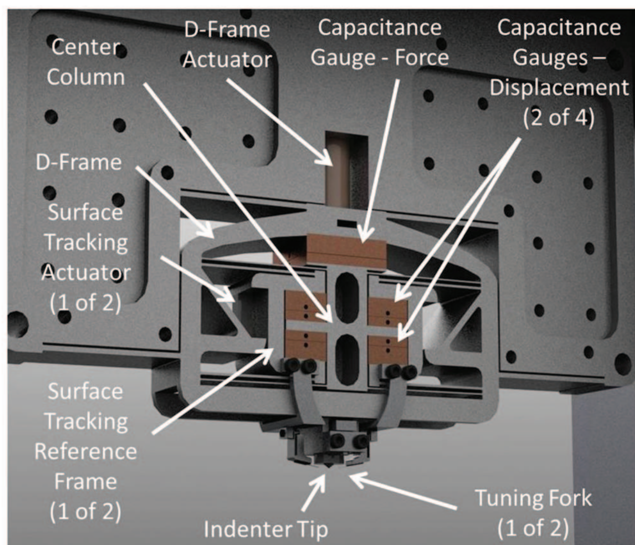

FIG. 2. A computer-assisted design rendering of the PNP load head, showing the critical components. Details of PNP operation are presented in the discussion related to Figure 3.

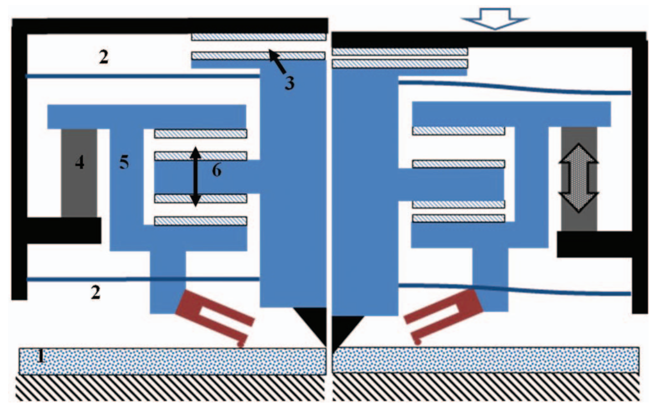

FIG. 3. Schematic representation of the operation of the PNP load head in surface tracking mode. On the left, the tuning fork has sensed the surface through a shift in its resonant frequency, and the indenter tip is positioned just above the specimen (1). On the right, the D-frame in the load head has advanced downward, the indenter tip has been pressed into the specimen, and the springs (2) supporting the indenter tip have deflected, allowing measurement of the applied force via the capacitance transducer (3). As the D-frame advanced, however, feedback to the piezoelectric actuator (4) held the displacement frame (5) fixed with respect to the specimen surface. Therefore, the capacitance gauges (6) make a direct measurement of the motion of the indenter tip with respect to the specimen surface that is not influenced by the compliance of the gantry, the X, Y, and Z axis translation stages, or any aspects of the specimen mounting scheme.

air). This shift in frequency, typically 0.2 Hz to 0.5 Hz for all specimens studied, is used in a feedback control system to maintain the position of each tuning fork relative to the sample surface directly beneath it. Each tuning fork locks to the surface independently, inherently adjusting for any tilting of the specimen. The indentation process is illustrated in detail in Figure 3, which shows only one-half of the symmetric mechanism. On the left, the tuning fork has sensed the surface, and is tracking its position, but the indenter tip has not yet reached the specimen surface. On the right, the D-frame has moved lower, through the extension of its piezoelectric actuator, and the indenter tip has penetrated the specimen surface. It is apparent from this diagram that the surface reference frame (5) has not moved relative to the specimen surface; feedback from the tuning fork circuit has caused its piezoelectric actuator (4) to extend so as to maintain a constant tuning fork resonant frequency, and hence a constant interaction distance and force between the tuning fork and the specimen surface. The force applied to the specimen by the indenter tip is determined by the deflection of the parallel springs (2) via the change in capacitance of gauge (3). The displacement of the indenter tip *relative to the surface reference tracking frame* is determined by the change in capacitance of the differential gauge (6). This displacement is identical to the penetration depth of the tip into the specimen (neglecting only the very small effects of the compliance between the indenter tip and center column). In actual operation, the two tuning forks and their respective reference frames track the surface independently and the displacement of the indenter tip, which is located collinearly with the tuning forks at the center point, is calculated from the average of the left and right displacements of the differential gauges. The capacitance gauges are of our own design and construction, and are guarded-plate

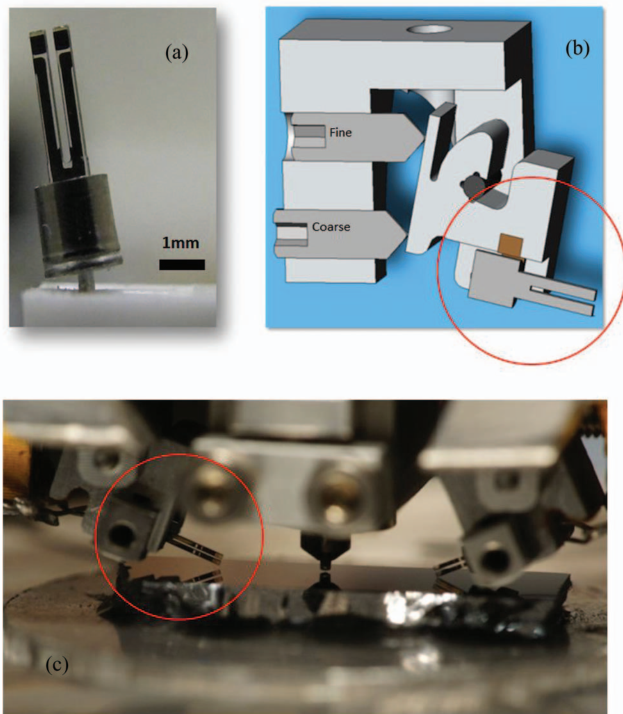

FIG. 4. Details of the tuning fork mounting and adjustment mechanism. (a) A close-up of a typical tuning fork. The cylindrical protective can has been cut and approximately two-thirds of it removed. (b) The pivot mechanism used to adjust the height of each tuning fork relative to the height of the indenter tip. Screws pressing against stiff and compliant regions of the adjuster provide both coarse and fine adjustment of tuning fork angle. (c) A photograph showing the indenter tip and tuning forks just above a specimen of single-crystal silicon. Circles are shown to indicate similar regions in (b) and (c).

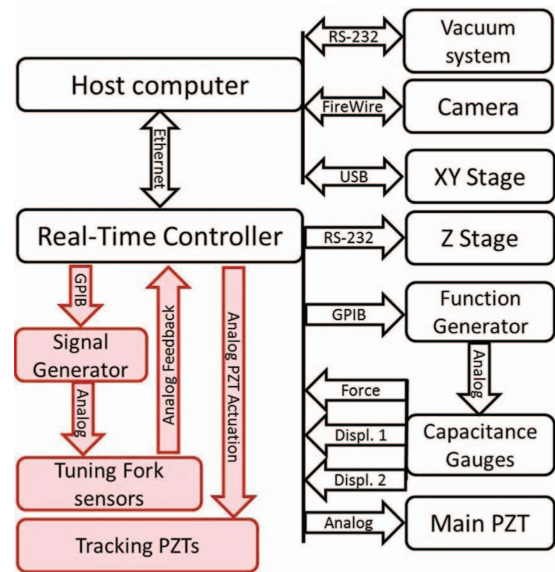

FIG. 5. A block diagram of the PNP control system. The feedback control system for tuning-fork surface tracking operation, consisting of a signal generator, the tuning fork sensors, tracking piezoelectric (PZT) actuators, and part of the real-time controller, is highlighted in red (with shading).

assemblies; the surfaces that form the capacitance gaps are diamond-turned. Details of their fabrication are presented in Ref. 18.

For the surface reference frame to track the surface properly, the relative heights of the two tuning forks and the indenter tip must be adjusted carefully, such that the initial interaction of the tuning forks with the surface occurs when the indenter tip is only a few micrometers above the surface. To achieve this, a sensitive adjusting mechanism was designed that enables precise vertical adjustment of the tuning fork relative to its reference frame. This mechanism, which incorporates coarse and fine adjusting screws, is shown in Figure 4, with close-up photograph of a tuning fork (Figure 4(a)), a solid model cross section of the adjustment mechanism (Figure 4(b)), and a photograph of the tuning forks and indenter tip positioned just above a single-crystal silicon specimen (Figure 4(c)). In Figure 4(a), it can be seen that the protective can that normally isolates the tuning fork from ambient air has been cut away such that approximately only the lower one-third of the cylindrical housing (which supports the base of the tuning fork) remains. This remaining section of can around the base facilitates the mounting of the tuning fork assembly in the adjustment mechanism shown in Figure 4(b).

Figure 5 is a block diagram showing the various electronic systems that control PNP operation. A variety of hardware interfaces are used to communicate between a host computer, a real-time controller, and the other system components. System components obtained from commercial suppliers contain embedded computers that are programmed over their respective busses and are indicated by the column of five blocks in the upper right of the figure. All other systems components are controlled using data acquisition systems housed in a PXI chassis. A critical part of the instrument is highlighted in red, with red background shading; this is the control loop that tracks each tuning fork response and moves the surface reference tracking frame relative to the D-frame to maintain a constant response on each tuning fork, and hence a constant distance between each tuning fork and the specimen surface. This control loop is implemented in a real-time LabVIEW program (National Instruments, Austin, TX) and has an effective bandwidth of ∼100 Hz, which is currently limited by the general purpose interface bus (GPIB) interface between the real-time controller and the signal generators. This system will soon be upgraded to the one that uses field-programmable gate array techniques to drive and detect tuning fork response; this will increase the speed of the control loop to a bandwidth that will be limited only by the mechanical response of the tuning fork itself.[19]

Measurements of capacitance and tuning fork frequency response are obtained by demodulation of amplified signals from AC bridge circuits. While the capacitance gauges provide a predominantly reactive load on a bridge arm, the combined inductance, capacitance, and resistance of the tuning forks makes bridge balancing more of a challenge. In this case, the bridge circuit for the tuning forks is driven by two synchronized sources from commercial function generators with amplitudes and phases being individually selected. Implementation of this method requires communication over a GPIB and forms the limitation on controller bandwidth mentioned above. Details of this technique will be prepared for a

future publication. All piezoelectric actuators are controlled using digital to analog converters for generating a control voltage for high voltage amplifiers.

III. INSTRUMENT ENVIRONMENT

Several aspects of the PNP design, particularly the surface-referenced displacement measurement, are intended to reduce the susceptibility of the instrument to environmental effects such as thermal gradients. Nevertheless, it is desirable to provide the best possible laboratory environment for the instrument.

The PNP laboratory is located on the ground floor of a NIST laboratory building, in a room where temperature is controlled to ±0.5 °C. The chamber sits on a heavy cast-iron optical table with three layers of vibration isolation between the table and the laboratory floor: one set of pneumatic isolators and two sets of elastomer isolators. Inside the chamber, the indenter assembly (base plate, gantry, translation stages, and load head) rests on a commercial passive vibration isolation table. The relative vibration amplitudes measured at the PNP load head (using the capacitance gauge that normally measures force) before and after these vibration isolation measures were taken are shown in Figure 6(a). The remaining peaks observed are primarily due to building air handling system (10 Hz) and resonances in the load head (150 Hz to 170 Hz).

Figure 6(b) demonstrates the benefit of the sealed chamber for controlling the temperature of the PNP. While the laboratory temperature fluctuated over nearly 1.0 °C on a time scale of tens of minutes due to cycling of the room's air cooling system, the temperature inside the chamber showed a maximum excursion of 0.02 °C, with a much lower rms variation. In this case the chamber was sealed, but contained air at ambient atmospheric pressure.

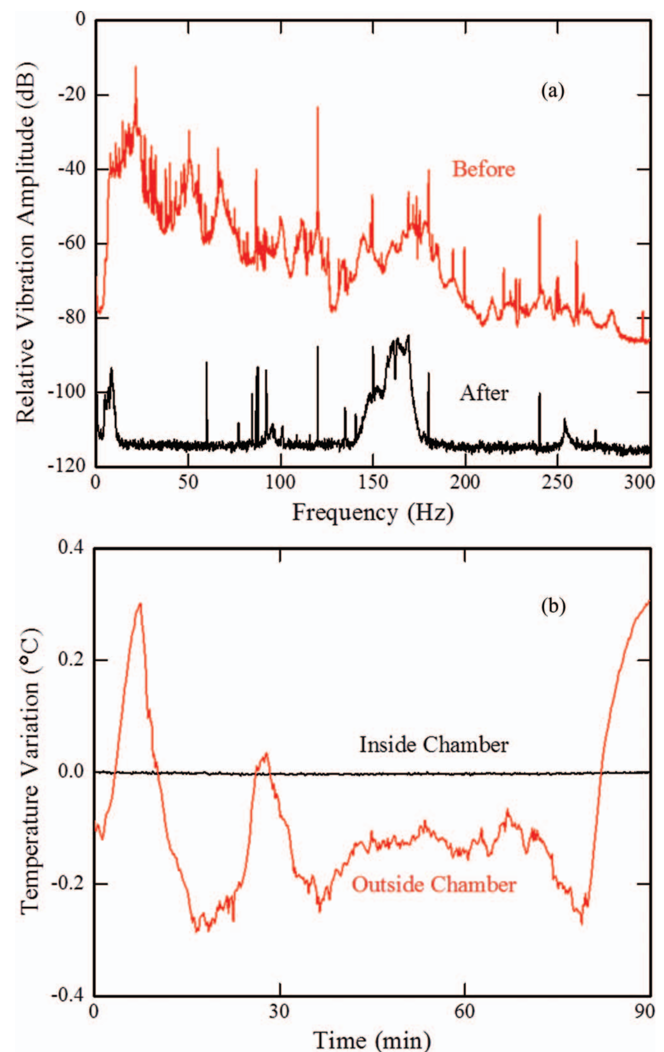

FIG. 6. Vibration and noise environment of the PNP. (a) Vibration spectra recorded by the PNP load head in the sealed chamber before and after the implementation of several vibration isolation measures. (b) Typical temperature variations observed inside and outside the sealed PNP chamber. The laboratory temperature is controlled to ∼±0.5 °C. The rms variation in temperature inside the chamber is less than 0.005 °C, with a maximum excursion less than 0.02 °C, over the same time period.

IV. INSTRUMENT PERFORMANCE

In this section, we describe calibration procedures and present experimental results that document several aspects of PNP performance, including the noise floors in the force and displacement data, the degree of thermal drift observed, and the effect of sample mounting compliance. In addition, we use the PNP to measure (a) the Young's modulus of fused silica, a material commonly used in the nanoindentation community as a reference material and (b) indentation creep of poly(methyl methacrylate) on time scales significantly longer than those normally accessible by conventional instrumented indenters.

A. Calibration, noise, and thermal drift

In day-to-day operation, both force and displacement are measured using the custom capacitance gauges and associated electronics described above. This means that calibration paths must be established that tie the output voltage of each capacitance gauge to the desired output data.

In the case of displacement, this was accomplished by mounting a laser-based, optical-fiber interferometer system of our own design in parallel with the capacitance gap to be calibrated. This interferometer system is described in detail in Ref. 20, but the basic technique involves the mounting of the cleaved end of an optical fiber opposite a reflecting surface (in our case a small piece of gold-coated silicon wafer) to create a Fabry-Pérot cavity approximately 100 μm to 200 μm long. The two optical fibers used to calibrate the capacitance gauges between the surface reference tracking frame and the D-frame can just barely be seen in Figure 1(a), taped to the outer frame of the load head. The precision and accuracy of the interferometer system far exceed the performance of the PNP capacitance gauges; the noise floor of the interferometer system is 2 pm rms and system accuracy is determined by the long-term accuracy and stability of the laser source, which is 1 pm on a nominal wavelength 1550 nm. Therefore, both the precision and accuracy of PNP displacement measurement is limited by the noise floor at the capacitance gauge output. The measured noise floor was 13 pm/$\sqrt{\text{Hz}}$ rms when the indenter

tip was not in contact with a specimen. This value was determined from an unfiltered, 10 000 sample, time sequence of capacitance gauge output voltage data taken with a 1 kHz sampling rate. When the Berkovich indenter tip was in contact with a silicon specimen, in servo-controlled surface tracking mode for a force of 5 mN, the noise level actually increased slightly, to 16 pm/$\sqrt{\text{Hz}}$ rms, presumably as a result of a small amount of noise introduced by the feedback circuitry.

To calibrate the lower end of the PNP force range, a passive force cell was employed that had been calibrated using NIST-traceable artifact masses. This force cell is designed specifically to mount in nanoindentation systems, in place of a specimen, such that the indenter tip presses directly on the force platen. It is capable of measuring a maximum force of 10 mN. Design and calibration of this force cell is described in Refs. 21 and 22 For forces in the range 20 μN to 10 mN, it has been shown to be accurate to within $\pm$ 0.2% for any applied force in that range, and to have a rms noise floor below 10 nN for calibration measurements of 1 s or longer. To calibrate forces greater than 10 mN, traceably calibrated masses were placed directly on the center column of the PNP load head. The values of these masses were known to much better than 0.01%. The noise floor for the force data reported by the PNP force transducer, determined using the same times series methodology as was used for displacement, was found to be 0.06 μN/$\sqrt{\text{Hz}}$ rms with the indenter tip away from the specimen surface and 0.12 μN/$\sqrt{\text{Hz}}$ rms under servo-controlled surface tracking conditions. Therefore, at very low forces, as with the calibration of PNP displacement data, the precision and accuracy of the PNP force data are limited by the PNP noise floor. Through an intermediate range of forces up to the 10 mN limit of the calibration force cell, accuracy is limited by the calibration cell. And finally, above 10 mN, force accuracy is well below 0.01%. This level of accuracy is valid all the way up to the maximum PNP force of 150 mN, because the noise floor of a few micronewtons holds all the way up to maximum force; there are no changes in gain or other electric adjustments required to span the full force range.

Because of the surface referencing design of the PNP, we expect it to be relatively immune to thermal drift errors, but long-term thermal drift effects were nevertheless characterized. Figure 7 shows the change in indentation depth observed with a diamond Berkovich indenter tip in contact with a single-crystal silicon specimen under a fixed 30 mN force. In such an experiment, silicon is not expected to show any creep behavior, so we expected indentation depth to remain constant if surface tracking was working properly. We observed that the indentation depth changed by only a few nanometers over a 12 h period, demonstrating a level of stability not achievable with instrumented indenters that do not employ surface referencing.

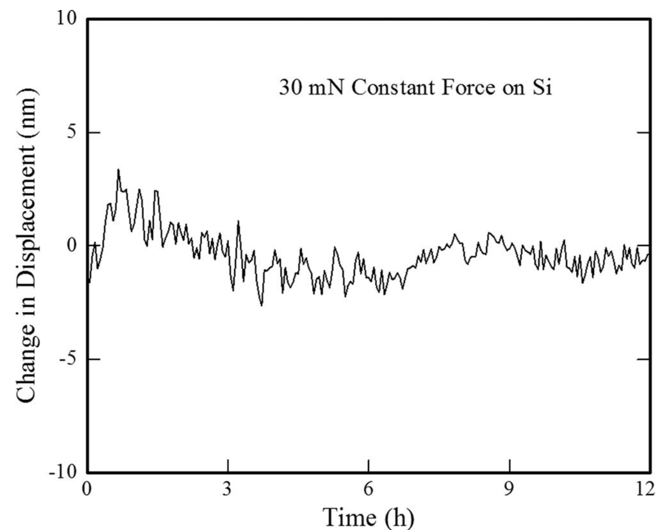

FIG. 7. The observed change in the position of a Berkovich indenter tip relative to the specimen surface while a constant indentation force of 30 mN was held for 12 h.

B. Effect of substrate compliance on force-displacement data

Instrumented indenters that measure displacement of the indenter tip relative to the load head rather than the specimen surface are susceptible to errors introduced by variation in the compliance of the specimen mount. The PNP, on the other hand, should be immune to such errors, even if the specimen mount is very compliant. To test this hypothesis, we indented the same fused silica specimen mounted in three very different ways. First, we mounted the specimen onto a solid aluminum cylinder using a thin layer of cyanoacrylate adhesive, a commonly used method in the nanoindentation community, and clamped the cylinder solidly to the Z translation stage identified in Figure 1(a). For the second test, we replaced the thin layer of glue with a 3 mm thick sheet of rubber gasket material, as shown in Figure 8(a). No adhesive was used—the gasket was simply placed on the aluminum cylinder and the fused silica was placed on the rubber gasket. Finally, as an extreme test, we replaced the rubber gasket with a 12 mm thick piece of very porous, open-cell polystyrene foam. The stiffness's of these three mounting configurations were measured directly by pressing on the silica surface with a flat-punch indenter tip having a radius of 10 μm. The dramatic differences in stiffness are shown in Figure 8(b).

After characterizing the stiffness of each mounting configuration, we then performed conventional Berkovich indentations on the fused silica for each configuration, using a 5 mN maximum force in each case, and compared the results. Figure 9(a) shows a comparison of the force-displacement data for the stiff glue mount and the rubber gasket. Blue solid lines are the glued mounting, dashed red lines are the rubber gasket mounting. Two different types of displacement are plotted versus force. The two curves that show the greatest displacement are the displacement of the D-frame for each test, relative to the outer frame of the load head. The two small-displacement curves are the indentation depth as measured with surface tracking. Although the stiffnesses of the two mounting configurations vary by a factor of almost 100, the reproducible force-depth data for the actual indentation demonstrates that the surface tracking is capable of negating the effects of significant compliance in the full frame of the instrument.

Figure 9(b) shows comparable results for the foam mount during which the indentation depth is less than 4% of the in-

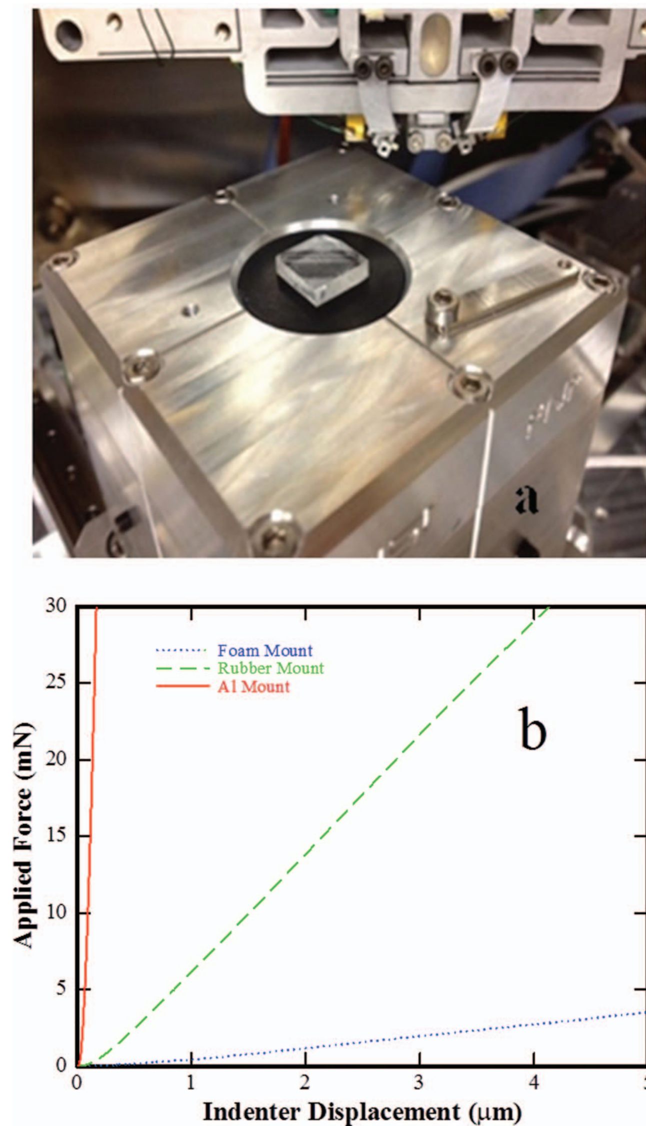

FIG. 8. (a) Photograph showing the fused silica specimen, 12 mm × 12 mm × 3 mm thick resting on 3 mm thick rubber gasket material. (b) The stiffness of three different mounts for the silica specimen, as measured with a circular flat punch 10 μm in diameter: silica glued to an Al cylinder with cyanoacrylate adhesive (red solid line), 546 mN/μm; silica resting on 3 mm thick rubber gasket (green dashed line), 7.4 mN/μm; and silica resting on 12 mm thick polystyrene foam (blue dotted line), 0.75 mN/μm.

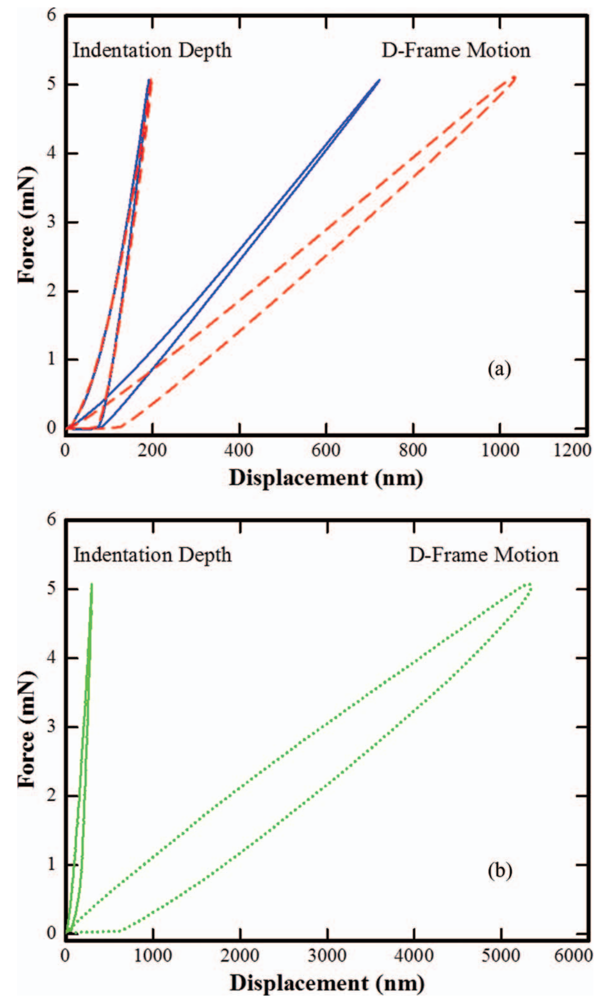

FIG. 9. (a) Force-displacement data from 5 mN Berkovich indentations on the silica specimen shown in Figure 8. Blue solid lines are for silica glued to an Al mount; red dashed lines are for silica resting on the rubber gasket. Although movement of the D-frame is significantly different for the two mounting methods, the indentation depth measured relative to the tuning-fork surface reference frame is correct even for the much more compliant rubber mount. (b) Force-displacement data for the silica specimen resting on polystyrene foam. Again, both D-frame motion and surface-referenced indentation depth are shown.

denter motion. In this case, although surface tracking dramatically improves the displacement data, a careful examination of the indentation "depth" data with surface tracking shows that it does not superimpose well with the depth data from the stiffer mounts; it reaches a maximum depth of 300 nm, while the correct indentation depth is just under 200 nm. This error is most likely to be related to a significant tilting of the specimen outside of tuning fork measurement plane, particularly if the two tuning forks are not perfectly collinear with the tip exactly halfway between them. This mounting is extreme, however, and unlike anything that would normally be encountered.

C. Indentation of fused silica

The performance of the PNP was further characterized by making a series of indentations on the fused silica specimen described above, using the stiffest mounting method—gluing the silica specimen directly on the Al cylinder. Here, we performed a series of Berkovich indentations at the same location using maximum forces that increased by 5 mN on each subsequent loading. The force-depth data are shown in Figure 10(a). Unlike standard "partial unloading" tests, in this experiment the indenter tip was completely withdrawn from the surface before reloading (hence the negative "indentation depth" shown), to test the reproducibility of the surface tracking.

The force-depth data were then analyzed to determine an experimental value of Young's modulus for the fused silica using a standard Oliver and Pharr power-law analysis[23] of each of the ten unloading curves. The first 75% of each unloading curve was used for the power-law fit, and a Poisson's ratio of 0.17 was assumed for the fused silica. The results, as a function of the calculated indenter contact depth for each maximum force, are plotted in Figure 10(b). The

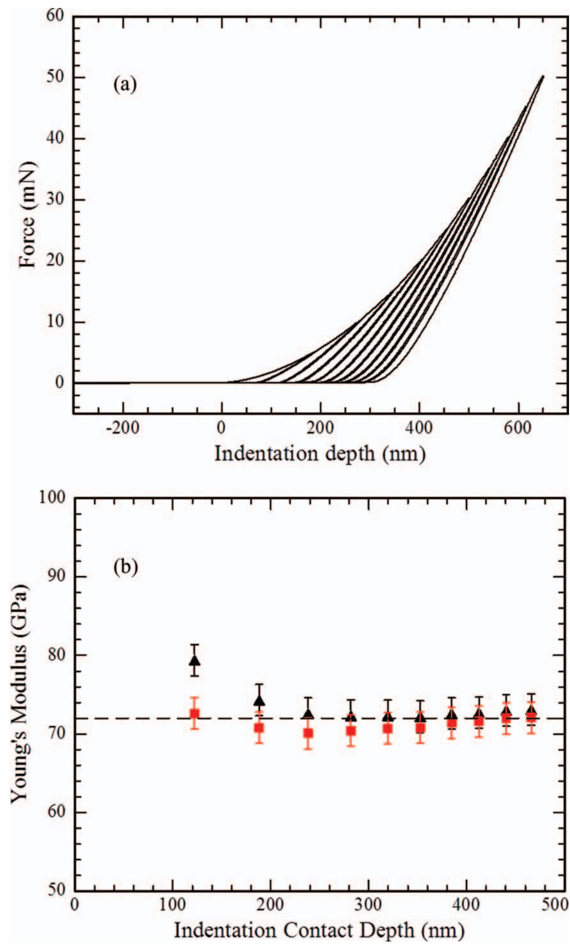

FIG. 10. (a) Force vs. indentation depth for Berkovich indentation of fused silica, measured with the PNP. Peak forces from 5 mN to 50 mN, in 5 mN steps, were applied sequentially, with the indenter tip fully retracted above the specimen surface prior to each reloading. (b) Young's modulus calculated from power-law fits to the individual unloading slopes in (a), assuming a Poisson's ratio of 0.17 for silica. The values represented by black triangles are calculated assuming a perfectly sharp Berkovich geometry; the red squares assume a rounding of the Berkovich tip with a radius of curvature of ≈50 nm. The dashed line is the literature value of 72 GPa. Error bars represent one standard deviation in the uncertainty of the unloading fits.

black triangles represent the modulus assuming that the diamond Berkovich indenter tip was a perfectly sharp pyramid, and show an increasing value of modulus at the shallowest indentation depths. Actual Berkovich tips invariably have some rounding of the tip as a result of the polishing processes used in tip fabrication. The assumption that the tip is perfectly sharp results in an underestimation of the contact area between tip and specimen for shallow indentation depths, and a resulting overestimation of the modulus, as observed. The addition of a small correction term[23] to account for tip rounding brings the results, now plotted with red squares, into better agreement with the literature value of 72 GPa (dashed line) across the full range of indentation contact depth. The error bars are determined by the uncertainty in the values of the power-law fit parameters determined from the unloading data.

D. Measuring indentation creep with the PNP

Nanoindentation can be used to measure the time-dependent behavior of small volumes of material, by making an indentation and then either (a) holding a fixed force while measuring the indenter tip creep deeper into the specimen or (b) holding a fixed indentation depth while measuring the force relaxation. However, instruments that do not incorporate surface tracking typically cannot measure creep reliably for time scales longer than a minute or two, because they typically have thermal drift rates of the order of 0.1 nm/s or greater that quickly introduce unacceptable error into the indentation depth data.[24] We have used the PNP's surface tracking capability to evaluate its ability to perform indentation creep experiments over a longer time scale. The very small amount of thermal drift we observe in the PNP, as presented above in Figure 7, demonstrates that our indentation depth data are reliable over long periods of time. In this current design, the tuning fork surface sensing imposes a nominally constant force on the specimen. Therefore, the surface reference frame will also experience creep behavior, the magnitude of which will depend on the stress introduced by the interaction of the tuning fork with the surface. In practice, the stress field produced by the proximity probe is difficult to quantify. However, we have been able to set an upper limit on the magnitude of the interaction force using the same low-force calibration cell described above in the calibration section. We mounted this cell under a tuning fork and closed the servo control loop between the tuning fork and the platen of the calibration force cell in the same way that we lock to specimen surfaces. Under this condition, no detectable force, either attractive or repulsive, is reported by the force cell. As discussed above, this cell has a noise floor of 10 nN, and applied forces only two to three times higher will produce a noticeable shift in its baseline output. We, therefore, conclude that the interaction force between the tuning fork and a sample surface under normal surface tracking control is no greater than 20 nN to 30 nN, and we believe that even with PMMA this interaction is not likely to produce significant specimen creep (relative to the displacements being measured at the indentation site) at the tuning fork locations. However, a more detailed study of this interaction is planned.

Figure 11 shows the indentation creep behavior of poly(methyl methacrylate) (PMMA) measured with the PNP using a Berkovich indenter. The bulk specimen measured 20 mm × 20 mm × 5 mm thick. In Figure 11(a), we show the indentation depth as a function of time for an indentation force that begins at zero at time $t = 0$ and reaches a maximum force of 5 mN at $t = 9.5$ s. From that point on, the force is held at 5 mN. In Figures 11(b) and 11(c), the abscissa origin has been shifted such that $t = 0$ now represents the time at which the force first reached 5 mN, and the ordinate now shows the *change* in indentation depth after that force was reached. For short times (Figure 11(b)), the creep behavior is very well characterized by a simple, empirical logarithmic function $\Delta D(t) = \mathrm{A}\ln(\mathrm{B}t + 1)$, where ΔD is the change in depth and A and B are fit parameters, suggesting that a single creep mechanism is at work. However, for times beyond about 20 min (Figure 11(c)), the observed creep rate changes significantly from that predicted by the original fit. Beyond 50 min, the data can again be fit with the same form of logarithmic function, with very different fit parameters, implying a change in the creep mechanism. Such an observation

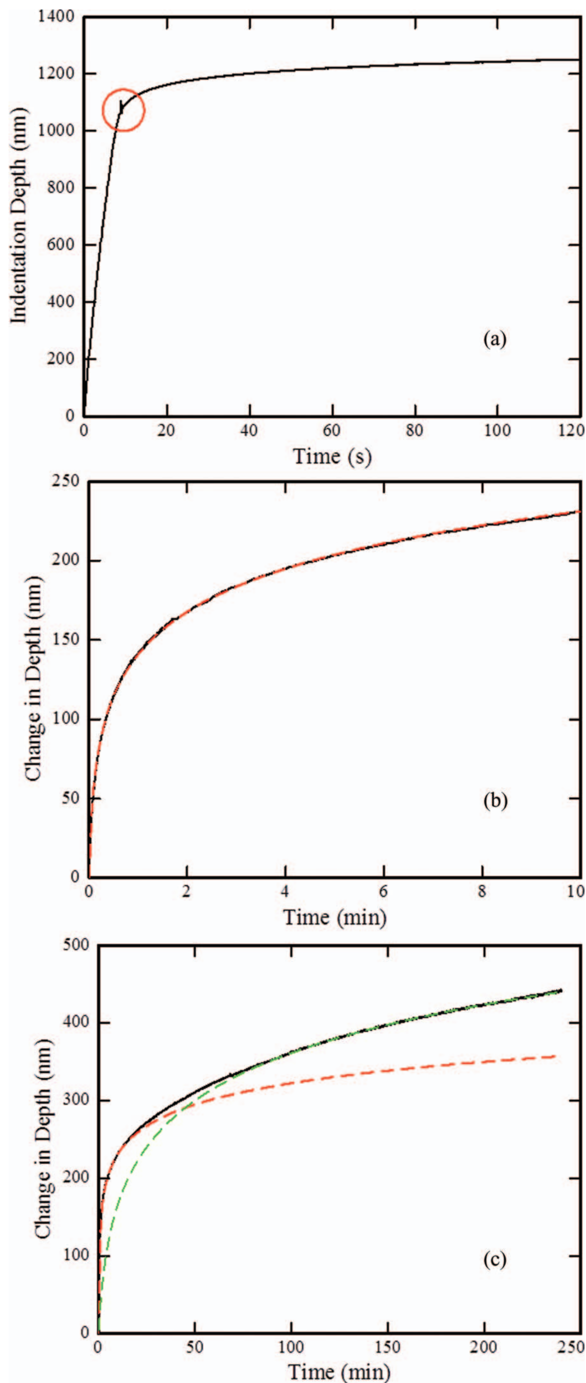

FIG. 11. Measurement of indentation creep in poly(methyl methacrylate) using a Berkovich indenter tip and a fixed applied force of 5 mN. In (a), time = 0 and depth = 0 correspond to the beginning of initial loading. The maximum force of 5 mN was reached after approximately 10 s (indicated by the circled spot) and the data show a slight noise deflection when the PNP switched to holding a fixed 5 mN force. Figures (b) and (c) show the change in indentation depth under fixed force, where time and depth now correspond to changes relative to the point in (a) where the force first reached 5 mN. The red curve in (b) and (c) is a logarithmic fit to the data over the first 10 min under full applied force, as described in the text, and the green curve in (c) is a logarithmic fit to the data after 60 min.

is consistent with the work of Yang *et al.*,[25] who use multiple exponential terms to obtain fits spanning the complete measurement duration. Such a transition could not be observed with most conventional nanoindenters.

V. SUMMARY

This paper presents the design and evaluation of a surface-referenced indentation platform capable of measuring penetration of an indenter into a specimen surface. As far as possible, this design aims to reduce the coincidence of the loop around which forces are transmitted from tip to specimen support from the reference frame that is necessary for measurement of relative translation between the specimen and the indenter. The major reason for adopting such a design is to reduce displacement uncertainty due to the effect of serial compliances of all elements of the instrument where the two loops coincide. Shortening of the measurement loop to a small region about the indenter also reduces temperature-induced displacement uncertainties. Additionally, dual displacement measurement centered on the indenter tip significantly reduces Abbé errors that also form a major component of displacement uncertainty in other instruments.

Surface sensing by servo controlling a proximity sensor to a constant height adds significant complexity in terms of mechanical implementation and noise. In practice, given free noise floors of 0.06 μN/$\sqrt{\text{Hz}}$ rms and 13 pm/$\sqrt{\text{Hz}}$ rms in force and displacement measurement, respectively, the system still maintains noise floors of 0.12 μN/$\sqrt{\text{Hz}}$ rms and 16 pm/$\sqrt{\text{Hz}}$ rms under closed loop control in contact with a specimen. Given the load and displacement ranges of 150 mN and 10 μm, respectively, and operating in a low-mechanical-noise environment, this platform is capable of providing measurements of interest spanning a broad range of nanoindentation studies.

In principle, the short measurement loop of this instrument should result in correspondingly low thermal expansion errors. Because most of the loop components are made from aluminum, temperature changes should have little effect on measured displacement. Given the measurement loop dimensions of around 30 mm and a coefficient of thermal expansion of 27×10^{-6} K^{-1}, a worst case displacement uncertainty is of the order 8 nm for variation of 1 K. This is consistent with stability measurements taken over 12 h or more in our current laboratory environment. Such an attribute extends the capability of this platform for longer term creep and load cycle studies. Using the tuning fork probes for proximity sensing raises the issue of the long-term influence of this sensing method on the surface of the specimen. Given the numerous physical, geometric, and dynamic effects, modeling of the interaction forces is complex. In an effort to address this issue, further experimental studies are ongoing, as is a redesigned indenter head that replaces the tuning forks with optical surface sensing.

By referencing from the specimen surface, compliances due to the specimen geometry and mounting method have little influence on measured indentation depth. This has been illustrated in a rather artificial manner by measuring an indentation on a specimen mounted on an unusually compliant support. Even in this case, for which displacements of the indenter are more than 100 times larger than the indentation depth, the results remain consistent with those obtained with more carefully controlled tests.

ACKNOWLEDGMENTS

This work was supported in part by funding from the National Institute of Standards and Technology (NIST) Innovations in Measurement Science program. Certain commercial equipment, instruments, or materials are identified in this paper in order to specify the experimental procedure adequately. Such identification is not intended to imply recommendation or endorsement by NIST, nor is it intended to imply that the materials or equipment identified are necessarily the best available for the purpose.

[1] K. Herrmann, N. Jennett, W. Wegener, J. Meneve, K. Hasche, and R. Seeman, Thin Solid Films **377–378**, 394 (2000).
[2] K. J. Van Vleit, L. Porchlik, and J. F. Smith, J. Mater. Res. **19**, 325 (2004).
[3] J. B. Pethica, R. Hutchings, and W. C. Oliver, Philos. Magn. **48**, 593 (1983).
[4] V. R. Howes, H. J. Goldsmid, and C. A. Baird, J. Phys. E: J. Sci. Instrum. **20**, 1507 (1987).
[5] L. Wieczorek, V. R. Howes, and H. J. Goldsmid, J. Mater. Sci. **21**, 1423 (1986).
[6] H. J. Goldsmid, V. R. Howes, and C. A. Baird, J. Mater. Sci. Lett. **6**, 1043 (1987).
[7] A. M. Daniel, S. T. Smith, and M. H. Lewis, Rev. Sci. Instrum. **65**, 632 (1994).
[8] J. Woirgard and J. C. Dargenton, Meas. Sci. Technol. **6**, 16 (1995).
[9] A. Shimamoto and K. Tanaka, Rev. Sci. Instrum. **68**, 3494 (1997).
[10] E. R. Coley, “A new instrument for nanoindentation,” M.S. thesis (University of North Carolina, 2000).
[11] J. D. Ellis, “Reducing frame stiffness dependency in nanoindentation,” M.S. thesis (University of North Carolina, 2007).
[12] S. T. Smith and J. D. Ellis, “Apparatus and method for surface property measurement with in-process compensation for instrument frame distortion,” U.S. patent 7,568,381 (5 August 2009).
[13] J. E. Sader, I. Larsen, P. Mulvaney, and L. R. White, Rev. Sci. Instrum. **66**, 3789–3798 (1995).
[14] J. L. Hutter and J. Bechhoefer, Rev. Sci. Instrum. **64**, 1868–1873 (1993).
[15] H.-J. Butt and M. Jaschke, Nanotechnology **6**, 1 (1995).
[16] J. Woirgard, B. Bellaton, and R. Consiglio, “Measuring head for nanoindentation instrument and measuring method using same,” International Publication number WO 2006/069847 A1 (2006).
[17] J. Nohava, N. X. Randall, and N. Conté, J. Mater. Res. **24**, 873 (2009).
[18] B. K. Nowakowski, S. T. Smith, and D. T. Smith, Proc. ASPE **50**, 97 (2010).
[19] K. Karrei and R. D. Grober, Ultramicroscopy **61**, 197 (1995).
[20] D. T. Smith, J. R. Pratt, and L. P. Howard, Rev. Sci. Instrum. **80**, 035105 (2009).
[21] J. R. Pratt, J. A. Kramar, D. B. Newell, and D. T. Smith, Meas. Sci. Technol. **16**, 2129 (2005).
[22] K.-H. Chung, S. Scholz, G. A. Shaw, J. A. Kramar, and J. R. Pratt, Rev. Sci. Instrum. **79**, 095105 (2008).
[23] W. C. Oliver and G. M. Pharr, J. Mater. Res. **7**, 1564 (1992).
[24] M. R. VanLandingham, N.-K. Chang, P. L. Drzal, C. C. White, and S.-H. Chang, J. Polym. Sci., Part B: Polym. Phys. **43**, 1794 (2005).
[25] S. Yang, W.-Y. Zhang, and K. Zeng, J. Appl. Phys. **95**(7), 3655 (2004).